Superstructure-based optimization framework to assess defossilization pathways in petrochemical clusters

Tan, Michael; Nikolic, Igor; Ramírez, Andrea Ramírez

DOI
10.1016/j.ces.2025.122783

Publication date
2026

Document Version
Final published version

Published in
Chemical Engineering Science

Chemical Engineering Science 321 (2026) 122783

Contents lists available at ScienceDirect

Chemical Engineering Science

journal homepage: www.elsevier.com/locate/ces

Superstructure-based optimization framework to assess defossilization pathways in petrochemical clusters☆

Michael Tan [a,*], Igor Nikolic [b], Andrea Ramírez Ramírez [c]

[a] Department of Engineering Systems and Services, Faculty of Technology, Policy and Management, Delft University of Technology, Jaffalaan 5, 2628BX Delft, the Netherlands
[b] Department of Multi-Actor Systems, Faculty of Technology, Policy and Management, Delft University of Technology, Jaffalaan 5, 2628 BX Delft, the Netherlands
[c] Department of Chemical Engineering, Faculty of Applied Sciences, Delft University of Technology, Van der Maasweg 9, 2629 HZ Delft, the Netherlands

ARTICLE INFO

Keywords:
Superstructure
Optimization
Petrochemical clusters
Carbon transition

ABSTRACT

The petrochemical industry must transition its material and energy sources from fossil-based sources to more sustainable alternatives. While decarbonizing the energy source is challenging, defossilization of the material feedstock is significantly more difficult. In this work, we present a superstructure-based, multi-period, multi-objective optimization framework to address this problem. This framework focuses on minimizing the use of fossil carbon and modifications to petrochemical clusters while explicitly controlling the order of appearance of new processes. The combination of process options becoming available to the solution space over time and the cluster being locked in a path-dependent transition allows the framework to capture realistic transformation pathways. We demonstrate the framework with a small-scale case study of 10 fossil-based and 6 alternative processes. The results demonstrate the ability of the framework to select optimal defossillization pathways while simultaneously considering the impacts on mass and energy flows across the cluster.

1. Introduction

The petrochemical industry needs to transform both its material and energy feedstock if it is to significantly reduce its greenhouse gas emissions by 2050. In recent years, changing the source of carbon feedstocks to alternative carbon sources (ACS) in refineries and the petrochemical industry has increasing gained attention. For example, Vogt and Weckhuysen (Vogt and Weckhuysen, 2024) envision that the current fossil-based carbon feedstocks (oil and natural gas) will be replaced with biomass, CO_2, and plastic waste by 2050.) Meng et al. (Meng et al., 2023) explored planet-compatible pathways for transitioning the chemical industry and found that in addition to alternative carbon sources (ACS), degrowth and circular strategies are required to reach net-zero emissions.

Several processes are being investigated to replace the production of fossil-based chemical building blocks (CBB) such as ethylene, propylene, and methanol and or the production of the end-of-value chain chemicals (EVC), like polyethylene terephthalate (PET), styrene monomer, and methyl *tert*-butyl ether (MTBE). The number of potential alternative processes is large, although many of them are still at early development stage. Manalal et al. (Manalal et al., 2025),for instance, identified 69 process routes to produce ethylene from ACS, 32 routes to produce methanol, 58 to produce propylene, and 38 to produce benzene/P-xylene. In order to select the most promising technologies or routes, the performance of individual ACS-based process routes is often compared with their fossil-based counterparts or with other green alternatives by using techno-economic and or life cycle assessments. Three examples of such comparisons are Zuiderveen et al. (Zuiderveen et al., 2024), who assessed alternative ways to produce benzene, toluene, and xylene, Liptow et al. (Liptow et al., 2015), who assessed the production of bio-based ethylene, and Kim et al. (Kim et al., 2021) focusing on the production of green propylene.

While defossilizing carbon feedstocks is, in theory, possible, it is far from straightforward in practice account. Defossilization will require modifications or replacement of existing processes, which will significantly impact existing value chains. Existing petrochemical processes are highly interconnected, allowing companies to decrease mass and energy losses and develop common infrastructure (e.g., energy or wastewater plants). Although such mass and energy interconnections exist in any cluster, they are often neglected when assessing the

☆ This article is part of a special issue entitled: 'M&SforSustainability' published in Chemical Engineering Science.

* Corresponding author.
E-mail address: m.d.tan@tudelft.nl (M. Tan).

https://doi.org/10.1016/j.ces.2025.122783
Received 14 January 2025; Received in revised form 8 September 2025; Accepted 11 October 2025
Available online 13 October 2025

performance and impact of ACS processes.

The transformation of these petrochemical clusters will occur over time, with a (gradual) step-wise transformation by removing or adding individual processes. Limitations on local or regional availability of resources (land, water, energy) further complicate the transformation. Given the highly complex interrelations, modeling and simulating the cluster impacts before embarking on investments is essential. Several modeling approaches have been used to examine the transition of the energy sector. The models typically use top-down or bottom-up approaches, such as integrated assessment models (IAMs) and agent-based modeling (ABM). IAMs use a top-down approach to investigate large-scale interactions between human and natural systems. In these IAMs, (sub)sectors of the energy sector, such as petrochemical clusters, are heavily aggregated. As a result, the changes that may occur to petrochemical clusters due to the transformation of the material feedstock are ignored in these models. ABM, on the other hand, uses a bottom-up approach to simulate the dynamic interactions of companies in an industrial park and how these interactions change over time. Han et al. (Han et al., 2022), for instance, used an ABM to investigate how external influences would affect cooperation among companies in an industrial park. ABM simulations focus on the behavior of the agents in a cluster and explore emergent structures but are not suited for designing optimal transition pathways. In addition, these models require extensive data to have the agents mimic the behavior of the companies in a petrochemical cluster and are computationally expensive as they require multiple simulations to explore all outcomes. Therefore, alternative methods that deal with the addition of processes over a sequence of time for exploring and evaluating transformation pathways to identify the optimal transformation of petrochemical clusters are needed.

Towards this end, methods like superstructure-based optimization have been used for comparing alternative process or equipment units. In this approach, an optimal design is chosen with respect to one or multiple objective functions (e.g., costs, emissions). The resulting optimization problem is implemented as a mixed integer linear program (MILP) or a mixed integer nonlinear program (MINLP). An area where optimization approaches are widely used is for the synthesis and design of new chemical processes (Mencarelli et al., 2020). Optimization has also been used to identify how *existing* industrial clusters could increase their performance by sharing waste heat, water, and materials between companies (Boix et al., 2015). However, they do not consider the potential introduction of new processes or feedstocks into these clusters. Valenzuela-Venegas et al. (Valenzuela-Venegas et al., 2020), for instance, used multi-objective optimization to find the optimal design of material and energy exchange networks of the Kalundborg and Ulsan industrial parks. The authors aggregated many flows and, for example, did not consider different types of steam or material composition. Pan et al. (Pan et al., 2016) used a MILP model to optimize the material exchange of the Jurong Island industrial cluster. Martelli et al. (Martelli et al., 2017) used a superstructure-based MINLP model to optimize the design of heat exchanger networks and utility systems for chemical processes. Kim et al. (Kim et al., 2010) created a detailed utility model that optimized a network of steam, water, and electricity utilities of the Yeosu Industrial Complex. The previous works focus on increasing the performance of existing industrial clusters, mostly in terms of material or energy efficiency. A radical transformation of existing industrial clusters is, however, largely overlooked in the literature.

Superstructure-based optimization has also been used for the designing of *new* industrial clusters. Kantor et al. (Kantor et al., 2015), for instance, used a source-sink representation for the demand and supply of material and energy for the processes of a hypothetical cluster. The authors applied a multi-objective optimization of economic and environmental functions to find optimal designs of the industrial cluster. Kantor et al. (Kantor et al., 2020) presented a mathematical formulation for optimizing the integration of material and energy in industrial clusters. In their approach, the authors used a source-sink approach for mass flows, while a heat cascade was implemented for energy flows. Granacher et al. (Granacher et al., 2022) implemented this framework as part of a digital twin for decision-making in the design of energy systems. This digital twin was used for the design of an integrated biorefinery. All these studies assume green field applications, ignoring the pre-existing conditions, connections, and processes in today's petrochemical clusters.

Finally, besides optimizing the mass and energy flows of industrial clusters, optimization models have also included temporal elements. Bishnu et al. (Bishnu et al., 2017), for example, used a multi-period optimization model to design water exchange networks for industrial clusters. In their model, the number of industrial processes increases over time, and the water exchange network adapts to it. Han et al. (Han et al., 2020) showed a multi-period optimization for the design of hydrogen networks among processes in industrial clusters. In both of these works, the authors noted the increased performance by performing the optimization over all timesteps of the model assuming the model had perfect foresight. Kuo and Chang (Kuo and Chang, 2014) used a similar multi-period optimization approach to optimize the design of hydrogen networks for seasonal variations. Due to the uncertainties associated with the development time-frame of novel processes, and the exact moment when novel ACS-based processes can be introduced into existing clusters, a step-wise approach is needed.

In this work, we aim to address these knowledge gaps by developing a superstructure-based optimization framework to identify optimal transformation pathways of petrochemical clusters. his optimization framework explicitly incorporates existing interconnections between petrochemical processes and considers the transformation in step-wise additions over time, where future options can be locked out by previous decisions The application of the framework is illustrated in a case study based on the Port of Rotterdam petrochemical cluster. In comparison to existing work, the process data is grounded in detailed Aspen Plus simulations of individual units, ensuring complete mass and energy balances. This article is structured as follows. In section 2, the mathematical framework developed to model the defossilization of a petrochemical cluster is presented. Section 3 describes the case study and the results of the framework application. In Section 4, the conclusions and future outlook are given.

2. Method

The goal of this work is to develop a superstructure-based optimization model that considers pre-existing material and energy connections of chemical and utility processes within petrochemical clusters, considers that processes can be added and removed step-wise over time, and has the ability to lock-out future option due to past choices. This optimization model is a multi-period multi-objective model that aims to identify configurations of processes and feedstocks for the defossilization of petrochemical clusters by implementing changes over a period of time.

2.1. Definition of the layers and nodes

To develop the model, a graph representation was used to set up the superstructure-based optimization model. In this representation, the nodes represent the available feedstocks, desired products, chemical processes, utility generation processes, energy sinks, and energy sources. The links in the graph illustrate potential interconnections between the different nodes. To distinguish between material and energy interconnections, the model used separate layers for material and energy flows. This approach allowed separate constraints to be enforced in each respective layer. A generic representation of the superstructure used is shown in Fig. 1, where the top part of the figure shows the material layer and the bottom is the energy layer.

The connections in the material layer are explicitly defined to match the pre-existing value chains in a petrochemical cluster. In the model, transfer nodes were defined to distribute the required chemical

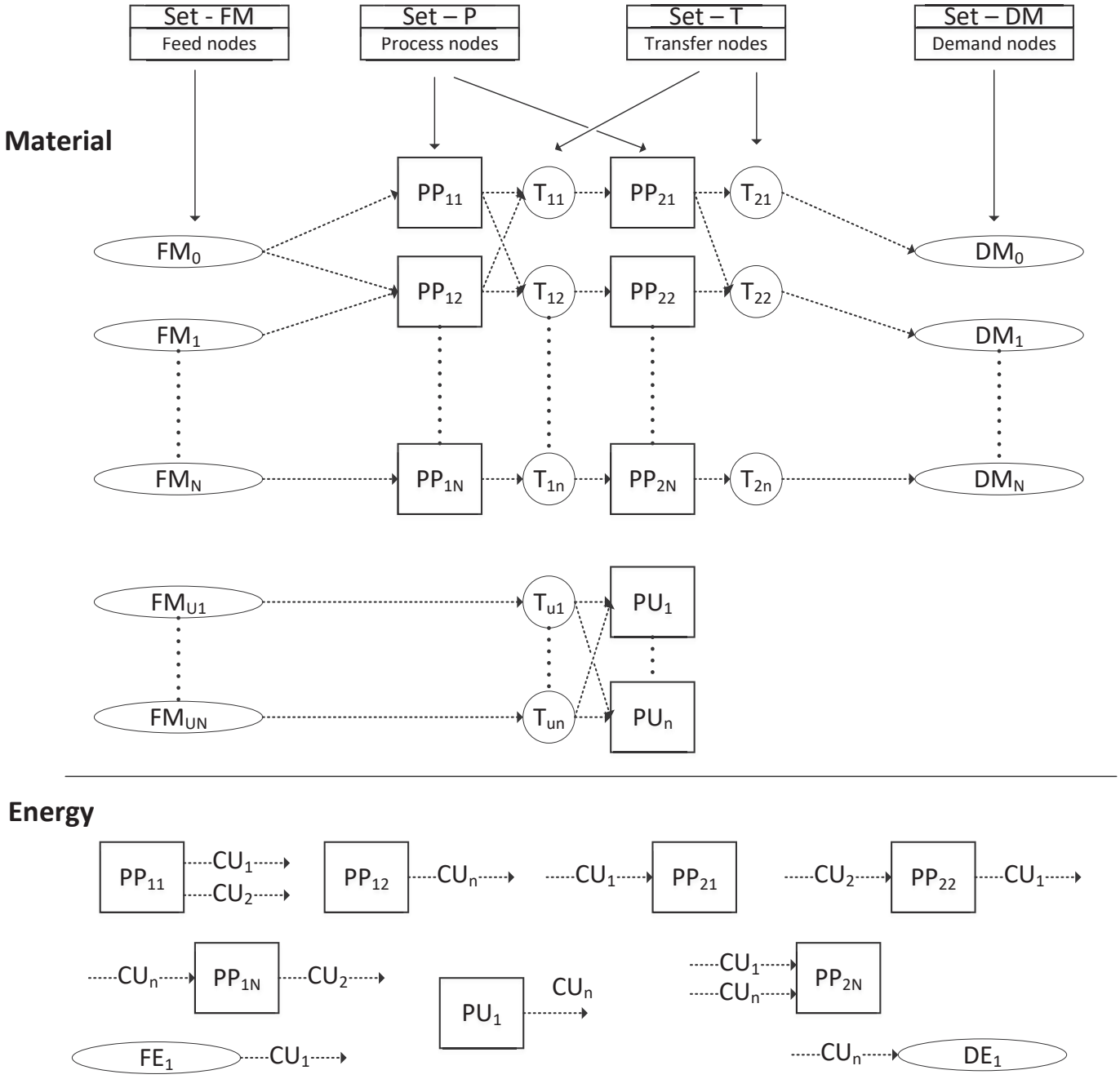

Fig. 1. Generic superstructure representation. In the figure, FM_n is a material feed node, FE_n is an energy feed node, PP_n is a chemical process node, PU_n is a utility process, T_n is a transfer node, DM_n is a material demand node, and DE_n is an energy demand node.

materials to the different process nodes and demand nodes. The model will select the optimal processing routes and optimal starting feedstocks to produce the required chemical products. In addition to the fossil-based processes from the existing value chains, the model also contains ACS-based processes, which can be disabled in the model to make them unavailable as a potential solution. This implementation is explained in more detail in subsection 2.4.3. For modeling the energy layer, the energy equations are solved based on the proximity of nodes to each other using an approach that matches the energy demand and energy supply. In contrast to the material layer, the links are not explicitly defined using transfer nodes. This approach allows all potential connections between nodes to be considered when closing the energy balance.

All nodes in the system belong to a set ***B***. The *transfer nodes* were grouped together (subset $\boldsymbol{T \subset B}$). The process and utility generation nodes were grouped together as *process nodes* (subset $\boldsymbol{P \subset B}$**).** The *process nodes* were further divided into *chemical processes* (subset $\boldsymbol{PP \subset P}$), and *utility generation processes* (subset $\boldsymbol{PU \subset P}$). The chemical processes were further subdivided into *fossil-based chemical processes* (subset $\boldsymbol{PP_{Fossil} \subset PP}$) and *ACS-based chemical processes* (subset $\boldsymbol{PP_{ACS} \subset PP}$). The subset of utility generation processes was further subdivided into *fossil-based utility generation processes that could generate heat and or electricity* (subset $\boldsymbol{PU_{Fossil} \subset PU}$) and *electricity only based utility generation processes* (subset $\boldsymbol{PU_{Electric} \subset PU}$). All the different process subsets convert material and/or utilities into other materials and/or utilities.

The product nodes and energy sink nodes were grouped together as *demand nodes* (subset $\boldsymbol{D \subset B}$). These demand nodes were divided into *material demand nodes* (subset $\boldsymbol{DM \subset D}$) and *energy demand nodes* (subset

DE*⊂*D). The demand for the end-of-value chain chemicals was enforced at the material demand nodes (i.e., the system should produce the chemicals demanded by the outside system) and they act as overflow nodes for other potential products. The energy sink nodes represent the export of excess energy to the outside system.

Similar to the material demand nodes, the material feed and energy source nodes were grouped together as *feed nodes* (subset ***F*⊂*B***), and divided into *material feed nodes* (subset ***FM*⊂*F***) and *energy source nodes* (subset ***FE*⊂*F***). The material feed nodes act as the carbon sources for the chemical processes, while the energy source nodes represent the import of energy into the system.

Additionally, chemical and utility components were defined in the model. For the material layer, chemical components ***CC*** (e.g., methyl *tert*-butyl ether, ethylene, propylene) were defined, while utilities ***CU*** (e.g., low-pressure steam, electricity, refrigerants) were defined for the energy layer.

Petrochemical clusters can consist of multiple cluster sites with one to several companies present per cluster site. Examples of such sub-clusters are, for instance, a chlorine cluster, an ethylene cluster, etc. These cluster sites can be physically separated by a significant distance, making it difficult to transport some energy flows (e.g., low-pressure steam) between cluster sites. To take this into account, in the model, energy streams are constrained to the nodes within a given subcluster site, while material streams can cross the subcluster site boundaries. For the subcluster sites, a new set ***CS*** was defined. Where the nodes present on a cluster site were grouped together as (subset $\boldsymbol{B_{CS}}\subset\boldsymbol{B}$).

2.2. Material equations

In Fig. 2, the standard data structure for the nodes and the process nodes is presented. Each node b in the material layer has a total material mass flow of component cc $\left(Mass_{b,cc}^{In}\right)$. This is estimated as a mass balance, i.e., it is calculated based on all material streams flowing into the node. Similarly, each node has a total material mass flow of component cc leaving the node $(Mass_{b,cc}^{Out})$. The total mass flow going into a node is calculated using Eq. (1). Where, $Streams_{i,b,cc}^{Mass}$ is the mass flow rate of component cc going from node i to node b. For material feed nodes, the mass flowrate into the nodes is calculated using Eq. (2), where $Feed_{f}^{Mass}$ is the mass flow rate of the available feedstock, $X_{f,cc}^{FeedComp}$ is the composition of the feedstock, f_f^I is the feed node integer indicating whether a feed node is present (a value of zero indicates the feed node is inactive while a value of one indicates is active).

$$Mass_{b,cc}^{In}=\sum_{i\in\boldsymbol{B},i\neq b}Streams_{i,b,cc}^{Mass}\quad\forall b\in\boldsymbol{B}\wedge b\notin\boldsymbol{F},\forall cc\in\boldsymbol{CC}\tag{1}$$

$$Mass_{f,cc}^{In}=Feed_{f}^{Mass}\cdot X_{f,cc}^{FeedComp}\cdot f_f^i\quad\forall f\in\boldsymbol{FM},\forall cc\in\boldsymbol{CC}\tag{2}$$

The mass flow rate out from a process node is based on the conversion of material in the node. This mass of transformed material is assumed to scale linearly based on the mass flow into the node. For each node, a limiting component cc^* was selected that scales linearly with the inputs and outputs of the process node. For instance, for the production of ethylene oxide, ethylene was selected as the limiting component. Besides the limiting component, processes also may have a demand for additional chemicals that are provided by other processes that are part of the superstructure. This demand is enforced by using Eq. (3), where $Mass_{p,cc^*}^{In}$ is the mass flow rate of the limiting component going into process node p and $X_{p,cc}^{Mass,In}$ is the material demand parameter of the process node. Other material demands that are not produced by processes within the superstructure, such as solvents, are determined using Eq. (4), where $X_{p,cc}^{Mass,In,Aux}$ is the auxiliary demand parameter.

$$Mass_{p,cc}^{In}=Mass_{p,cc^*}^{In}\cdot X_{p,cc}^{Mass,In}\quad\forall p\in\boldsymbol{P},\forall cc\in\boldsymbol{CC}\tag{3}$$

$$Mass_{p,cc}^{In,Aux}=Mass_{p,cc^*}^{In}\cdot X_{p,aux\_sp,cc}^{Mass,In,Aux}\quad\forall p\in\boldsymbol{P},\forall cc\in\boldsymbol{CC}\tag{4}$$

Therefore, the mass out of a process node p is given by Eq. (5), where $X_{p,cc}^{P}$ is the conversion parameter of the process node. In addition to the main products, every process produces several streams of by-products and waste materials that are not shared with other nodes and are, therefore, not part of the connections in the superstructure. The mass flow rate of a by-product stream sp is calculated using Eq. (6) and the mass flow rate of waste stream sw is determined using Eq. (7).

$$Mass_{p,cc}^{Out}=Mass_{p,cc^*}^{In}\cdot X_{p,cc}^{P}\quad\forall p\in\boldsymbol{P},\forall cc\in\boldsymbol{CC}\tag{5}$$

$$Mass_{p,sp,cc}^{Out,Side}=Mass_{p,cc^*}^{In}\cdot X_{p,sp,cc}^{P,Side}\quad\forall p\in\boldsymbol{P},\forall cc\in\boldsymbol{CC}\tag{6}$$

$$Mass_{p,sw,cc}^{Out,Waste}=Mass_{p,cc^*}^{In}\cdot X_{p,sw,cc}^{P,Waste}\quad\forall p\in\boldsymbol{P},\forall cc\in\boldsymbol{CC}\tag{7}$$

The mass out of demand node d is given by Eq. (8), where d_d^i is the demand node integer indicating whether the demand node is present (the demand node is absent with a value of zero and present with a value of one). For other types of nodes in the model, such as transfer nodes, there is no conversion of material, therefore, the material flow into a node is equal to the material flow out of the node as given in Eq. (9).

$$Mass_{d,cc}^{Out}\cdot d_d^i=Mass_{d,cc}^{In}\quad\forall d\in\boldsymbol{DM},\forall cc\in\boldsymbol{CC}\tag{8}$$

$$Mass_{b,cc}^{Out}=Mass_{b,cc}^{In}\quad\forall b\in\boldsymbol{B}\wedge b\notin\boldsymbol{D}\wedge b\notin\boldsymbol{P},\forall cc\in\boldsymbol{CC}\tag{9}$$

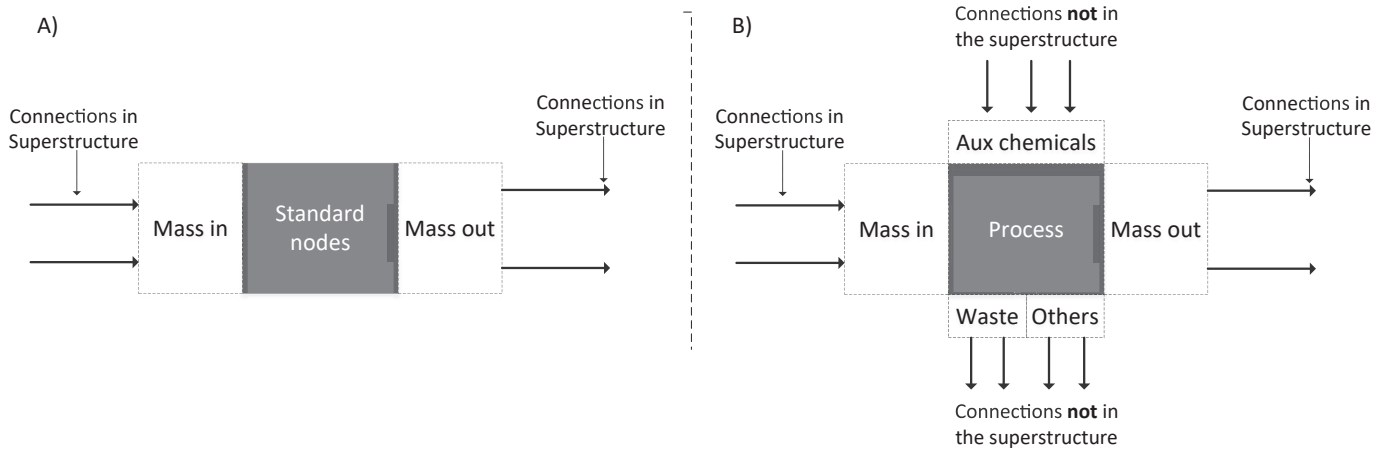

Fig. 2. Schematic of the data structure for the nodes (except process nodes) and for the process nodes.

As pointed out before, the purpose of the transfer nodes is to distribute chemicals among the material demand nodes and the processes requiring those chemicals. The mass flow rate of a component subset *cc* between transfer node subset *t* and node subset *j* is calculated using Eq. (10), where $y_{t,j}$ is the transfer coefficient. To make sure that the total mass flow rate of the links leaving the transfer node does not exceed mass out of the transfer node, an additional constraint is introduced (Eq. (11)). For the other nodes, the mass flow of a component *cc* in a link going from node *b* to node *j* is calculated using Eq. (12). In this equation, a separation factor $S_{b,j,cc}$ is used to distribute the fraction of each component in $Mass^{Out}_{b,cc}$ to the outgoing links going from node *b* to node *j*.

$$Streams^{Mass}_{t,j,cc} = Mass^{Out}_{t,cc} \cdot y_{t,j} \quad \forall j \in \boldsymbol{B}, \forall t \in \boldsymbol{T}, \forall cc \in \boldsymbol{CC} \tag{10}$$

$$\sum_{j \in \boldsymbol{B}, j \neq t} y_{t,j} = 1 \quad \forall t \in \boldsymbol{T} \tag{11}$$

$$Streams^{Mass}_{b,j,cc} = Mass^{Out}_{b,cc} \cdot S_{b,j,cc} \quad \forall b \in \boldsymbol{B} \wedge b \notin \boldsymbol{T}, \forall j \in \boldsymbol{B}, \forall cc \in \boldsymbol{CC} \tag{12}$$

Furthermore, each chemical process node was assumed to have an operating window. The lower and upper boundary of the production capacity was set using Eq. (13) for the fossil chemical processes and Eq. (14) for the ACS-based processes. Where, $K^{Flex}_{p,fossil}$ is a capacity flexibility parameter of the fossil processes and $K^{Flex}_{p,fossil}$ is the capacity flexibility parameter of the ACS-based processes. These capacity flexibility parameters are defined as the fraction that the process can deviate from its nominal production capacity. For instance, with a value 0.1, a process can downscale its production by 10 %. p^I_p is the positive process integer value, where if a process is not present, a value of zero is given, and where any positive integer indicates the number of times that a process is present in the cluster (for instance, three plants producing methanol). $K^{Cap}_{p,cc}$ is the nominal production capacity of component *cc* of process *p*. The bounds of the process decision variable are set using Eq. (15), where $p^{I,LB}_p$ and $p^{I,UB}_p$ are the lower and upper bounds of p^I_p, respectively.

$$\left(1 - K^{Flex}_{p,fossil}\right) p^I_p \cdot K^{Cap}_{p,cc} \leq Mass^{Out}_{p,CC} \leq p^I_p \cdot K^{Cap}_{p,cc} \quad \forall p \in \boldsymbol{PP}_{Fossil}, \forall cc \in \boldsymbol{CC} \tag{13}$$

$$\left(1 - K^{Flex}_{p,ACS}\right) p^I_p \cdot K^{Cap}_{p,cc} \leq Mass^{Out}_{p,CC} \leq p^I_p \cdot K^{Cap}_{p,cc} \quad \forall p \in \boldsymbol{PP}_{ACS}, \forall cc \in \boldsymbol{CC} \tag{14}$$

$$p^{I,LB}_p \leq p^I_p \leq p^{I,UB}_p \tag{15}$$

Finally, a chemical production demand is enforced on the material demand nodes of chemicals at the end of each value chain using Eq. (16). This chemical production demand is the export demand for the end-of-value chemicals (e.g., MTBE and styrene monomer) in the model.

In Eq. (16), K^{Tol}_d is the tolerance parameter of the lower boundary and $X^{Demand}_{f,cc}$ is the existing production rate of chemical *cc*. In the current version, the model is allowed to exceed the base export demand by 20 %. However, it is possible to run the model with lower or higher percentages.

$$\left(1 - K^{Tol}_d\right) \leq \frac{Mass^{Out}_{d,CC}}{X^{Demand}_{d,cc}} \leq 1.2 \quad \forall d \in \boldsymbol{D}, \forall cc \in \boldsymbol{CC} \tag{16}$$

2.3. Energy equations

In the energy layer, all chemical process and utility generation nodes have an energy demand and supply. The energy demand $Energy^{Demand}_{p,cu}$ for utility *cu* is calculated based on the mass flow rate going into the node of the limiting component $Mass^{In}_{p,cc^*}$ in the material layer and is given by Eq. (17). In this equation, $X^{Demand}_{p,cu}$ is a utility demand parameter relating the demand for a utility *cu* to $Mass^{In}_{p,cc^*}$.

$$Energy^{Supply}_{p,cu} = Mass^{In}_{p,cc^*} \cdot X^{Supply}_{p,cu} \quad \forall p \in \boldsymbol{P}, \forall cu \in \boldsymbol{CU} \tag{17}$$

The energy supply of the chemical process utility generation nodes is based on the mass flowrate of the limiting component and is given in Eq. (18), where $X^{Supply}_{p,cu}$ is a utility supply parameter.

$$Energy^{Demand}_{p,cu} = Mass^{In}_{p,cc^*} \cdot X^{Demand}_{p,cu} \quad \forall p \in \boldsymbol{P}, \forall cu \in \boldsymbol{CU} \tag{18}$$

In addition to the chemical process and utility generation nodes in the model, each cluster site has an energy source node and an energy sink node. The energy sink node acts as the outgoing energy connection which exports excess energy outside the system boundaries of the cluster, while the energy source node acts as the incoming energy connection for importing energy into the cluster. To ensure that, for a given cluster site *cs*, the model does not simultaneously import and export the same utility flow, an additional binary variable p^i_{cs} was introduced. The energy supply for the energy source and energy demand for the energy sink nodes were determined using Eqs. (19) and (20).

$$Energy^{Supply}_{f,cu} = f_{f,cu} p^I_{cs} \quad \forall f \in \boldsymbol{FE}, \forall cu \in \boldsymbol{CU} \tag{19}$$

$$Energy^{Demand}_{d,cu} = d_{d,cu}\left(1 - p^I_{cs}\right) \quad \forall d \in \boldsymbol{DE}, \forall cu \in \boldsymbol{CU} \tag{20}$$

Based on the energy supply and energy demand of nodes in a cluster site, the total site energy demand and supply of a utility *cu* was calculated using Eqs. (21) and (22).

$$Energy^{Total,Supply}_{cs,cu} = \sum\nolimits_{i \in \boldsymbol{B}_{cs}} Energy^{Supply}_{i,cu} \quad \forall cs \in \boldsymbol{CS}, \forall cu \in \boldsymbol{CU} \tag{21}$$

$$Energy^{Total,Demand}_{cs,cu} = \sum\nolimits_{i \in \boldsymbol{B}_{cs}} Energy^{Demand}_{i,cu} \quad \forall cs \in \boldsymbol{CS}, \forall cu \in \boldsymbol{CU} \tag{22}$$

For each cluster site, the total energy balance of utility *cu* is closed using Eq. (23), thereby making sure that the total energy demand matches the supply within a cluster site cs_n.

$$Energy^{Total,Supply}_{cs,cu} = Energy^{Total,Demand}_{cs,cu} \quad \forall cs \in \boldsymbol{CS}, \forall cu \in \boldsymbol{CU} \tag{23}$$

Like the mass of materials between the model nodes, we would like to track the flow energy between nodes. Therefore, a variable $Streams^{Energy}_{i,b,cu}$ was added that represents the flow of energy from a node *i* to a node *b* for utility *cu*. This variable is determined using Eq. (24), which is an energy balance over node b, ensuring that the inflow and outflow are in balance. Next, a constraint was added that enforces that the total flow of energy of utility *cu* leaving node *b* does not exceed the node's total energy supply of utility *cu*.

This constraint is set using Eq. (25).

$$Energy^{Supply}_{b,cu} + \sum\nolimits_{j \in \boldsymbol{B}_{cs}} Streams^{Energy}_{j,b,cu} = Energy^{Demand}_{b,cu} + \sum\nolimits_{j \in \boldsymbol{B}_{cs}} Streams^{Energy}_{b,j,cu} \in \boldsymbol{CU}, \forall b \in \boldsymbol{B}_{cs} \quad \forall cs \in \boldsymbol{CS}, \forall cu \tag{24}$$

$$\sum\nolimits_{j \in \boldsymbol{B}, j \neq b} Streams^{Energy}_{b,j,cu} \leq Energy^{Supply}_{b,cu} \quad \forall b \in \boldsymbol{B}, \forall cu \in \boldsymbol{CU} \tag{25}$$

Following the approach used for the chemical process nodes, each utility generation process was assumed to have an operating window. This operating window was enforced on the utility generation nodes using Eq. (26).

$$\left(1 - K^{Flex}_p\right) p^I_p \cdot K^{Cap}_{p,cu} \leq Energy^{Suply}_{p,cu} \leq p^i_p \cdot K^{Cap}_{p,cu} \quad \forall p \in \boldsymbol{PU}_{Fossil} \quad \forall cu \in \boldsymbol{CU} \tag{26}$$

2.4. Multi-period multi-objective optimization

2.4.1. Objective functions

The model described in the previous section allows the evaluation of several objective functions, such as environmental and economic performance indicators. To illustrate this, we examine two objective functions, but similar equations can be formulated for other indicators. As the main goal of the model is to investigate the transformation of petrochemical clusters to the use of alternative carbon sources, the first objective function corresponds to the minimization of fossil-based carbon sources. This minimization is given in Eq. (27), where m_f^{Carbon} is the mass fraction of carbon in the fossil-based carbon feedstock f.

$$\min \quad \sum_{f \in \boldsymbol{FM}_{FC}} Feed_f^{Mass}\, m_f^{Carbon} \tag{27}$$

To illustrate the possibilities of the model, the second objective was to minimize the amount of new investments in the cluster while minimizing changes to the cluster. The two objective functions imply that in this case, the model will aim to identify configurations that use ACS while minimizing stranded assets. The second objective function is given by Eq. (28), in which stranded assets are minimized by including a penalty term. This objective function does not minimize costs, it minimizes what we call a "capex penalty", that is, the economic loss associated with stopping the use of current assets plus the new investment required by the new technologies. In the equation, the first term represents the penalty for removing an existing fossil-based process from the cluster. The second term represents the penalty for removing an existing fossil-based utility process, and the third term represents the costs involved in deploying a new ACS-based process in the cluster. In this equation, $CAPEX_p$ is the total capital expenditure required for the construction of a process p.

$$\begin{aligned}\min \Bigg(& \sum_{p \in \boldsymbol{PP}_{Fossil}} \left(1 - p_p^I\right) CAPEX_p + \sum_{p \in \boldsymbol{PU}_{Fossil}} \left(1 - p_p^I\right) CAPEX_p \\ & + \sum_{p \in \boldsymbol{PP}_{ACS}} p_p^I \cdot CAPEX_p + \sum_{p \in \boldsymbol{pp}_{ACS}} p_p^I \cdot CAPEX_p \Bigg)\end{aligned} \tag{28}$$

Using the two objective functions, a Pareto front is generated. It shows the trade-offs between the different solutions of the multi-objective model. There are several ways to construct Pareto fronts, with the ε-constraint method being one of the most well-known methods (Mavrotas, 2009). In the ε-constraint method, the model is optimized for a single objective function, while the other objective functions are implemented as additional constraints. In this work, the augmented ε-constraint method AUGMECON2 (Mavrotas and Florios, 2013) was used to generate the Pareto fronts.

2.4.2. Evaluation of the solutions

In the model, the solutions of the Pareto front are ranked using the Technique for Order of Preference by Similarity to Ideal Solution (TOPSIS) method (Hwang and Yoon, 1981). This method ranks the solutions based on their distance from the ideal and the non-ideal solution between 0 and 1, with the best solution being the closest to 1. The ideal and non-ideal solutions are a combination of the best and worst values of the considered criterion, respectively.

To apply TOPSIS, the desired decision criteria and their associated weights must be defined. Besides the key performance indicators used as objective functions for the creation of the Pareto front, other or alternative KPIs can also be introduced as assessment criteria. In this work, the objective functions used to create the Pareto front were also used to rank the solutions in TOPSIS. The weights allow a decision criteria to be preferred over the others, e.g., prioritizing defossilizing feedstocks over the associated costs. This approach allows to prioritize the solutions that are closer to the best value associated with that decision criteria.

2.4.3. Multi-period implementation

Two different strategies for solving the model were implemented, with both methods following identical procedures. In the multi-step method, ACS-based processes were added to the solution space over several steps, thereby increasing the number of potential solutions with each step. In the single step method, all potential ACS-based processes are introduced in the model in one single step, thereby allowing the global best solution to be identified as if all options were available at the same time. The multi-step method can be used to identify pathways to reach the configuration of the selected global solution. It allows to identify potential lock-ins introduced by the order in which technologies are deployed. For the model to consider changes that have occurred in a prior step, the following assumptions were made:

- The model has no perfect foresight. It does not know what processes are available in future steps and therefore, only evaluates the potential solutions based on the technologies available on the current step.
- Removed fossil-based processes cannot return in later steps.
- ACS-based processes that are introduced in a step cannot be removed later. This is done to avoid that the model will deploy a plant to just remove it a couple of years later.

In the appendices, Fig. A.1. shows the flowchart developed for solving the model in a multi-step, multi-objective optimization manner. First, the baseline fossil-based petrochemical cluster needs to be loaded as a starting point for the model. In each time step of the model, ACS-based processes are added to the solution space of the model. This is done by unlocking the process integer variable value associated with the ACS-based model from a value fixed to "0" and allowing the variable to be evaluated as part of the optimization. Next, a Pareto front for the time step is generated using the augmented ε-constraint method (AUGMECON2). This is shown in Fig. 3a. Each solution in this Pareto front is ranked using the TOPSIS method (see Fig. 3b). One could allow a decision maker to decide on the best solution among the top-ranked solutions of the Pareto front using an interactive modeling approach. However, in the current implementation, the solution ranked highest by TOPSIS is selected by the model as the best solution. This best solution is then loaded into the model, allowing all variable values associated with this cluster configuration to be accessed.

In the next step of the multi-step multi-objective model, the state of the cluster is updated. First, the process decision variable of each process $p_p^{I,n}$ is stored and compared to the process decision variable $p_p^{I,n-1}$ of the previous time step. This difference Δp_p^I, is calculated using Eq. (29).

$$\Delta p_p^I = p_p^{I,n} - p_p^{I,n-1} \tag{29}$$

For every process where Δp_p^I is not 0, the lower or upper bounds of p_p^I are adjusted. If Δp_p^I is negative, it indicates that one or multiple instances of the process have been removed in the latest timestep. In the current implementation, only fossil-based processes can be removed or changed. As we assume that removed fossil-based processes cannot return at later time steps, for the next time step, the upper bound of the process decision variable is adjusted to be equal to the current value of p_p^I.

$$p_p^{I,UB} = p_p^{I,n} \tag{30}$$

If Δp_p^I is positive, it indicates that one or multiple instances of the process have been added in the latest time step. Assuming that ACS-based processes cannot be removed in later timesteps, the lower bound of p_p^I is adjusted for the next time step using Eq. (31).

$$p_p^{I,UB} = p_p^{I,n} \tag{31}$$

After the cluster state has been updated, the model proceeds to the next

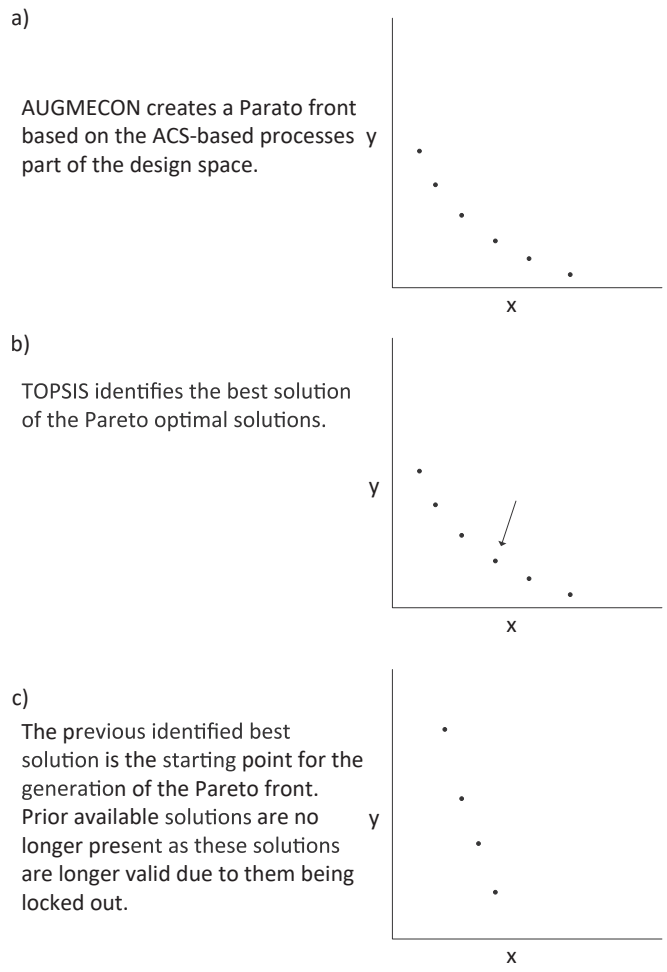

Fig. 3. Evolving Pareto front.

time step, where a new Pareto front is generated (Fig. 3c) and the whole procedure is repeated. Once the model has finished the final time step, it has determined the transformed petrochemical cluster configuration.

3. Illustrative case study

To illustrate the model capabilities to evaluate potential routes to defossilize petrochemical clusters, it was tested on a case study based on the petrochemical cluster in the Port of Rotterdam. To do this, an in-house model of the fossil-based model of the petrochemical cluster) was used. The model was described in detail in previous work (Tan et al., 2024). This model contains the mass and energy flows and interconnections, which are obtained from process plant-based Aspen Plus models (for each chemical process and utility process). The process models were designed using data of the process technology and production capacity of the existing fossil-based processes in the Port of Rotterdam. This real-world data was combined with data from literature to construct highly detailed the Aspen Plus models. In Table A.1. of the Appendices, an overview of all the processes, their production capacities, underlying data and assumptions is provided.

An overview of the superstructure representation of the case study based on this representative petrochemical cluster is presented in Fig. 4. Ten fossil-based processes (red boxes without outline in Fig. 4) and five utility generation processes (green boxes in Fig. 4) were selected as the starting point of the case study. An overview of all the processes, their main products, and production capacities is presented in Table 1.

Next, six ACS-based processes were added to defossilize the cluster. These processes and their production capacities are given in Table 2 and are shown as red boxes with a green outline in Fig. 4. Five processes provide ACS-based routes to produce four chemical building blocks, namely methanol, ethylene, propylene, and benzene. The ACS processes for these chemical building blocks are CO_2 hydrogenation to methanol, electrochemical reduction of CO2 to ethylene, methanol to aromatics (MTA), methanol to olefins (MTO), and plastic pyrolysis. The plastic pyrolysis process includes a hydrogenation step to saturate the pyrolysis oil and remove chlorine and sulfur. In addition to these alternative routes, an alternative route for producing an end-of-value chain chemical (MTBE) was also included. This route is based on the conversion of biomass to isobutylene via organosolv. Each of these ACS-based processes was assigned to the cluster site where the fossil-based process was located that they intended to replace. For instance, the MTO process was assigned to the same cluster site as the olefins process. As each of these processes consumes different forms and qualities of energy, several different energy types were defined for the case study. They include low-pressure steam (LPS), high-pressure steam (HPS), electricity, and cooling water.

Table 3 shows the main products and the respective demand that the model needs to fulfill. The introduction of ACS-based processes may result in lower demand for chemical building blocks and in a loss of the production of intermediate chemicals. In addition, the ACS-based processes may have completely different side-products compared to the fossil-based processes. Therefore, to allow for radical transformation, the model is only required to match the current production rate of the end-of-value chain chemicals that are present in the fossil-based configuration of the case study. For comparison of the product distribution, the produced chemicals are allocated to production categories based on Table 4.

The model was run using the two optimization approaches (see Table 5) described in the methodology (section 2.4.3). The order in which processes became available in the multi-period approach was based on the current TRLs of each ACS-based process. Therefore, in the first step, plastic pyrolysis (TRL 9) was made available to the design space. In the second step, CO_2 hydrogenation, MTA, and MTO (TRL 6–7, 7, 8–9) were added. In the third and final step, biomass to isobutylene (TRL 6–7) and direct electrochemical reduction of CO_2 to ethylene (TRL 3–5) became available.

In addition to these two optimization approaches, the model was run using two different settings for the process flexibility parameter K_p^{Flex} for the fossil-based processes. This flexibility parameter sets the lower operating window of each process. In the first setting, the capacity flexibility parameter was set to 0.1, thereby allowing an operating window between 90 %-100 % relative to the standard process production capacity of the fossil-based processes. In the second setting, the capacity flexibility parameter was set to 0.5, thus allowing an operating window of 50 %-100 % for the fossil-based processes. The capacity flexibility parameter was set to zero for the ACS-based processes to limit these processes to always operating at their maximum capacity.

Finally, the model also allows us to examine how limitations on feedstock availability can influence the pathways selected. To test this, a fifth run was performed where the availability of plastic waste as carbon feedstock was limited to 5000 ktonne/y with all other model input matching Run A.

The case study was implemented as a MILP in Pyomo 6.6.1 (Hart et al., 2011; Bynum et al., 2021) and solved using Gurobi 11.0.0 (Gurobi Optimization, 2024).

3.1. Defossilized petrochemical cluster

Fig. 5 presents the generated Pareto fronts for the model runs and the solutions selected via TOPSIS (indicated by arrows in the figure). From Fig. 5 it can be observed that about. 50 % of the fossil carbon could be replaced with 20 % of the costs required to reach a 100 % replacement of fossil carbon.

Fig. 4. Superstructure representation of the case study.

Table 1
Fossil-based process specifications.

	Process name	Process' main product(s)
	Chemical processes	
O1	Olefins	Ethylene Propylene
E1	Ethylene oxide	Ethylene oxide
E2	Ethylbenzene	Ethylbenzene
E3	Ethylene glycol	Ethylene glycol
M61	Tert-butyl alcohol dehydration	Isobutylene
M6	Methyl *tert*-butyl ether	Methyl *tert*-butyl ether
P11	C_4 Isomerization	Isobutane
P1	Propylene oxide/Tert-butyl alcohol co-production	Propylene oxideTert-butyl alcohol
P3	Propylene glycol methyl ether	Propylene glycol methyl ether
P6	Propylene oxide/Styrene monomer co-production	Propylene oxideStyrene monomer
	Utility processes	
U1	Steam methane reformer	Hydrogen
U2	Air separation unit	Oxygen
U3-IS, U3-SL	Natural gas-fired combined heat and power	SteamElectricity
U6-A, U6-I1, U6-I2	Natural gas-fired boiler	Steam

Table 2
ACS-based processes specifications.

	Process name	Process main product(s)
BM61	Biomass to isobutylene via organosolv	Isobutylene
CM1	CO_2 hydrogenation	Methanol
CO1	Electrochemical reduction of CO_2 to ethylene	Ethylene
MA1	Methanol to aromatics	Benzene o-Xylene p-Xylene
MO1	Methanol to olefins	Ethylene Propylene
PO1	Plastic pyrolysis	Naphtha, Diesel, Vacuum gas oil

Table 3
Products and their minimum production demand in the model.

Product	Product demand [ktonne/year]
Ethylene glycol	112.6
Methyl *tert*-butyl ether	385.5
Propylene glycol methyl ether	89.6
Styrene monomer	666.3

Table 4
Allocation of chemicals to production categories.

Product category	Chemicals
Methanol	Methanol
Ethylene	Ethylene, Ethylene oxide, Ethylene glycol
Propylene	Acetone, Propylene, Propylene glycol methyl ether, Propylene oxide,
C4	Isobutane, Isobutylene, Methyl *tert*-butyl ether
Benzene	Benzene, Ethylbenzene, Styrene
Xylene	o-Xylene, p-Xylene
Utility	Hydrogen, Oxygen
Heavy hydrocarbons	Naphtha, vacuum gas oil, diesel

Table 5
Performed model runs with their capacity flexibility for the fossil-based processes.

Run ID	Optimization mode	K_p^{Flex}
Run A	Global multi-objective	0.1
Run B	Multi-period multi-objective	0.1
Run C	Global multi-objective	0.5
Run D	Multi-period multi-objective	0.5

Allowing for capacity flexibility in production capacity affects the Pareto fronts. The two Pareto fronts with 10 % flexibility (Fig. 5a and Fig. 5b) have additional solutions that are not present on the Pareto fronts with 50 % flexibility (Fig. 5c and Fig. 5d). These additional solutions are configurations where a CO_2 hydrogenation plant to methanol is implemented to replace fossil-based methanol. These configurations are not Pareto optimal for the 50 % flexibility runs. The results also show that the Pareto front for the 50 % flexibility shifted to the left by operating some of the fossil processes at a lower capacity, thereby lowering the fossil-based carbon feedstock without requiring any further increase of costs.

When comparing the selected solution in the single-step model (Run A and Run C), identical configurations are selected for both cases, although the run with 50 % flexibility has a slightly lower operating capacity for achieving (slightly) higher defossilization of the petrochemical cluster. This same behavior is also observed for the multi-step runs, where for Run B and D, identical processes were selected with a slightly higher defossilization share in Run D. However, while the final configuration is identical for the two multi-step runs, the interim Pareto and the solutions selected by TOPSIS were different. Therefore, the model provides insights into the influence of parameters such as flexibility in the configurations of the model outcomes.

Finally, note that the lock-in of transformation pathways can be observed when comparing the Pareto fronts of the multi-step and single-step implementation (Fig. 5c and Fig. 5d). The Pareto front of run C

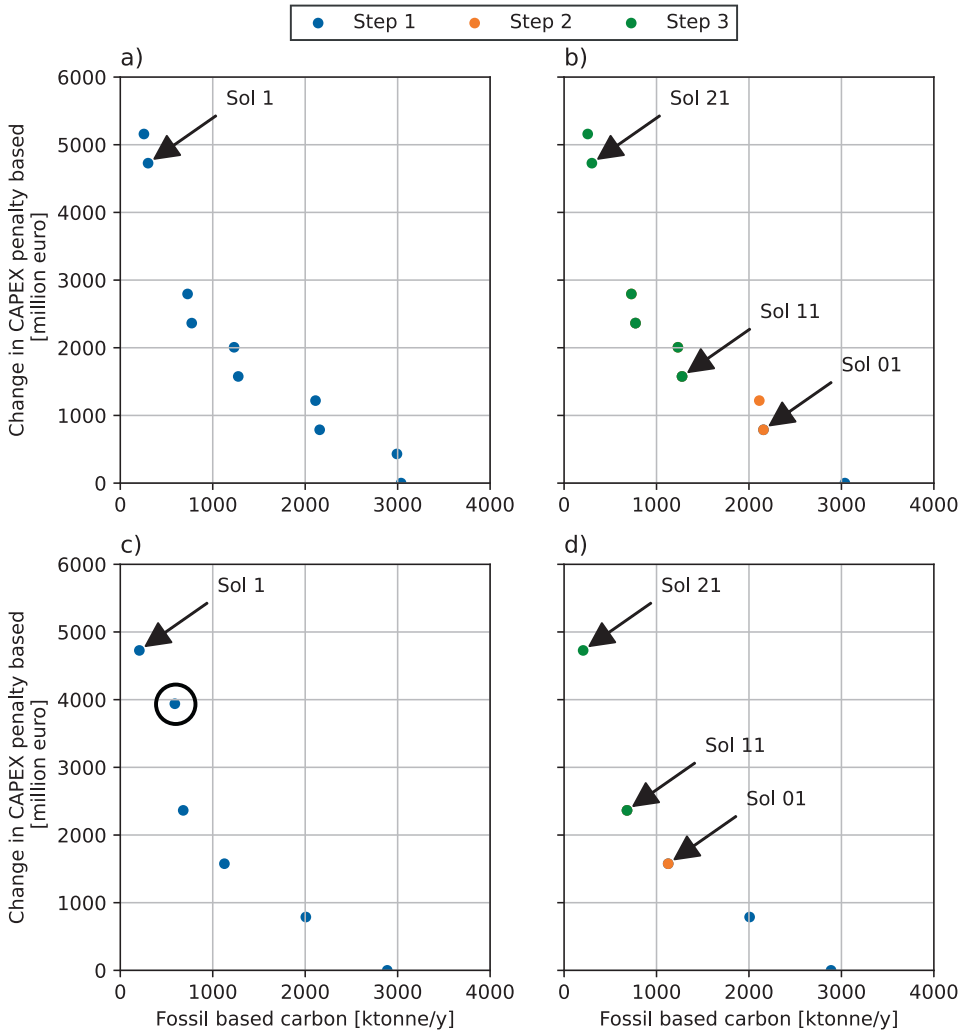

Fig. 5. Pareto fronts of the different model runs and their selected solutions by TOPSIS. a) Single-step at 10% flexibility. b) Multi-step at 10% flexibility. c) Single-step a 50% flexibility. d) Multi-step at 50% flexibility.

shows an additional solution that is not present on the Pareto front of run D. The cluster configurations that were selected during the modeling steps of the multi-step implementation of Run D locked the cluster into a transformation pathway. This lock-in, removed potential alternative cluster configurations, such as the cluster configuration shown in run C, from later modeling steps of run D.

3.1.1. Selected processes

The model allows detailed access to the solutions and provides insights into the type of technologies selected in and across pathways. In the case study, for instance, the results show that across the different runs, three plastic pyrolysis plants (PO1) and one biomass to isobutylene via organosolv process (BM61) are always selected by the model. The model also shows which fossil-based processes were fully replaced in all the runs: the PO/TBA (P1), Isomerization (P11), and TBA dehydration (M61). In addition to removing these fossil-based processes, two boilers that used waste streams from the P1 and P11 processes were also removed from the cluster in the four runs. These removals resulted in a relatively large increase of costs for a small gain in defossilization. For a complete list of all the processes, the number of plants for each process, and their relative operating capacity, see Table A.2. in the appendices.

Furthermore, it is notable that the remaining fossil-based chemical processes operate at their full capacity in the runs. The two exceptions are the olefins process and the SMR. The olefins process (O1) is scaled down in the four runs, as at full capacity, it would produce more ethylene and propylene than is required in the case study. Similarly, the SMR unit (U1) also scaled down its production to 90 % in runs A and B, and 53 % in runs C and D to minimize the production of excess H_2.

3.1.1.1. Changes to carbon feedstocks. Fig. 6 shows changes in the source of the carbon feedstock over the different steps. Note that the carbon source is expressed in ktonne of carbon embedded in each material. The results clearly indicate that although the sources of carbon change in the runs, there is a significant increase in the total amount of carbon (irrespective of its origin), from 3.3 Mt carbon in the base case to 14.7 Mt carbon in the defossilized cases. In other words, the cluster is not only defossilizing but also significantly recarbonizing. Note that in none of the model runs, full defossilization was achieved, which was to be expected as the case study focuses on the defossilization of chemical processes, and options to defossilize utilities, including the SMR, were not included in the case study. In the case of the SMR, for instance, it is assumed that the existing SMR unit would still be in operation, and only additional H_2 would be imported into the cluster if the H_2 produced by the SMR at full capacity is not enough.

The results in Fig. 6 show that in all cases, plastic waste was selected as the main carbon source to replace fossil carbon. Plastic waste is used as a carbon source for a plastic pyrolysis plant, which produces plastic-based naphtha, which can be used as an alternative carbon source to the

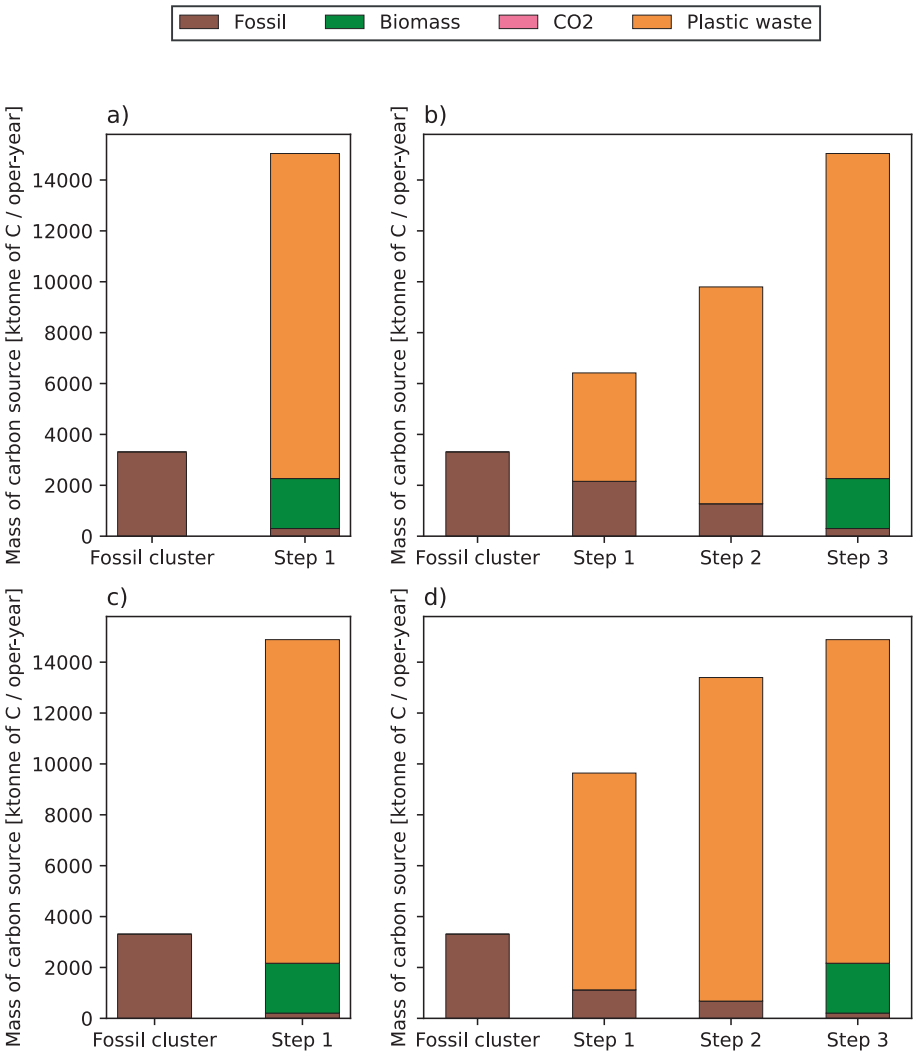

Fig. 6. Origin of the carbon feedstock selected by the model for the different model runs. a) Single-step at 10% flexibility. b) Multi-step at 10% flexibility. c) Single-step at 50% flexibility.. d) Multi-step at 50% flexibility.

fossil-based naphtha from the refinery. Besides plastic waste, biomass was selected as carbon feedstock to produce isobutylene via the organosolv process for the selected configuration of the single-step runs and selected for the final configurations of the two multi-step runs. In none of the runs, CO_2 was selected as a carbon feedstock. In the 50 % flexibility runs, Fig. 5C and D, configurations that include CO_2 as a feedstock are not Pareto optimal. In the two 10 % flexibility runs, configurations that include CO_2 as feedstock were found to be Pareto optimal, but the increase in costs required for a relatively small defossilization gain was too large to be selected by the model.

Fig. 6 also shows that while the two multi-step runs include three plastic pyrolysis plants by the end of the run, their interim configurations differ. In the 10 % flexibility solution, an additional plastic pyrolysis plant is selected in each step, while in the 50 % flexibility solution, the deployment is faster with two plastic pyrolysis plants being selected in the first step and a third one in the second step. The model opts for this in the 50 % run as the olefins can operate at a lower production capacity, which in combination with the two plastic pyrolysis plants, results in an almost complete defossilization of the naphtha feeding the olefins plant. When examining the remaining fossil-carbon feedstock, the results of the 50 % flexibility parameter have a smaller remaining fossil-carbon contribution due to the downscaling of the SMR unit.

3.1.1.2. Changes to product distribution. Fig. 7 shows the product distribution and how it changes at different steps. As a constraint, any run must match the production rate of the end-of-value chain chemicals (EVCs) in the fossil cluster. Therefore, the model can remove or replace processes that produce chemical building blocks and intermediate chemicals if they are no longer required for EVCs production. This will affect the mix of products exported from the cluster into the market. It was observed that for the selected ACS processes, the total mass of products increases with increasing levels of defossilization. The main difference between the fossil-based configurations and the final

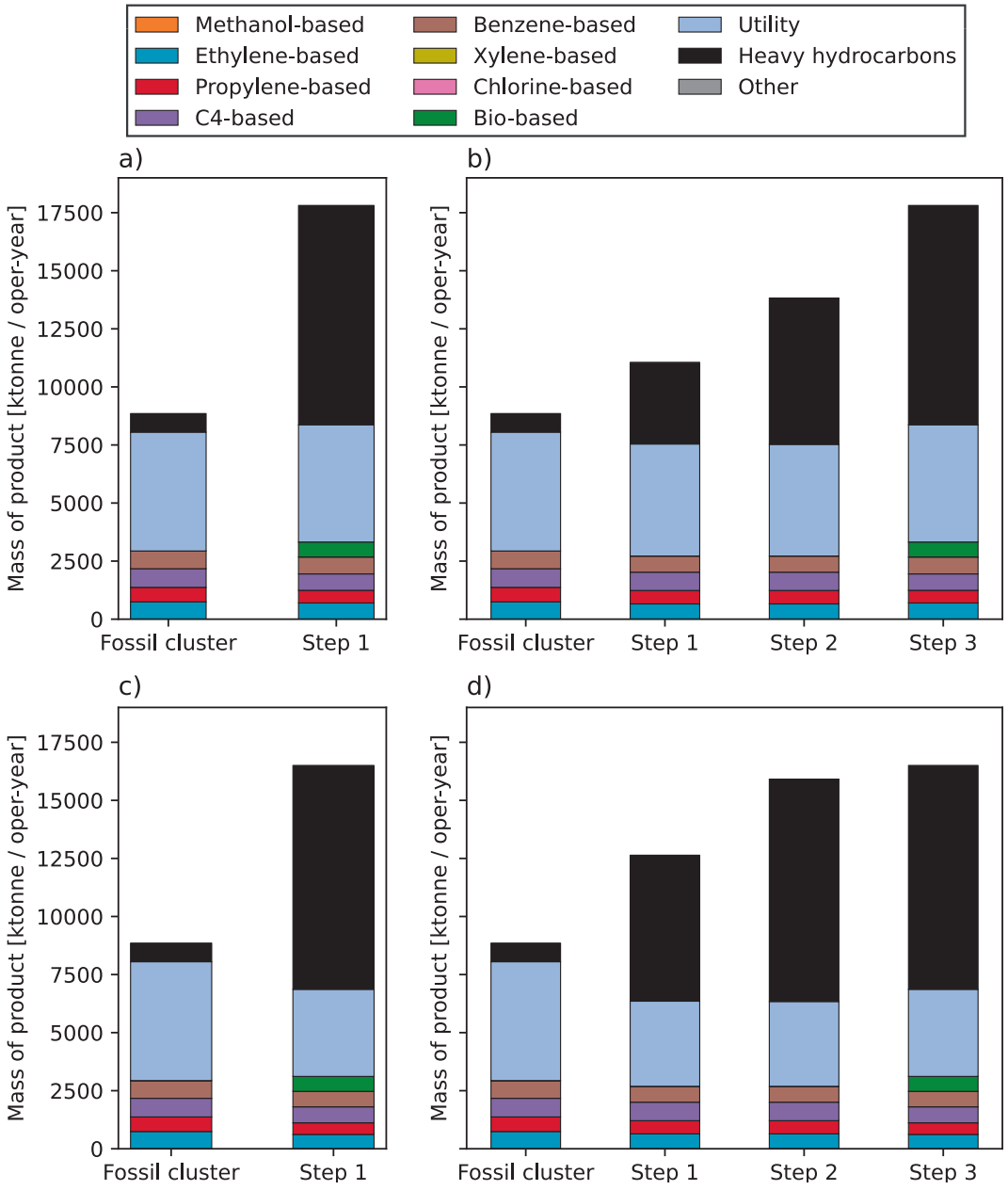

Fig. 7. The product distribution for the different model runs at different levels of defossilization. a) Single-step at flexibility parameter at 10% b) Multi-step at flexibility parameter at 10% c) Single-step at parameter at 50%. d) Multi-step at parameter at 50%.

solutions is the addition of a large fraction of heavy hydrocarbons. These heavy hydrocarbons are excess naphtha and side products of the plastic pyrolysis plants, namely diesel and vacuum gasoline oil. In addition, CO_2 is included (the bio-based category) to the materials exported from the cluster. As the plastic pyrolysis plants produce more naphtha than is required by the olefins plant, it is exported from the cluster. Biogenic CO_2 is a byproduct from the biomass to isobutylene process and is emitted from the cluster as it is not used as a material feedstock, in the selected model configurations and there was no carbon capture and storage included in the current runs in the model.

As indicated previously, the processes selected in the final configuration of the petrochemical cluster are identical across the four model runs. The resulting product distribution also very closely matches. There are, however, two differences between the 10 % flexibility parameter runs (A and B) and the 50 % in runs C and D. First, the 50 % flexibility runs have a larger fraction of excess naphtha that is exported from the cluster. Second, the 50 % flexibility runs have a smaller fraction of utility products (e.g., H_2 and O_2) that are exported from the cluster, due to the SMR unit operating at 53 % of its capacity.

3.1.1.3. Energy imports. As expected, defosilizing carbon feedstocks will affect the overall energy demand of the cluster. Fig. 8 show the distribution of the total energy imported per type. Similar to the results of the carbon feedstock and product distributions, the energy distribution also shows very similar energy distribution across the different model runs. The removal of the two boilers only results in a minor decrease in natural gas consumption as these boilers use waste streams as their primary source of energy. Adding a plastic pyrolysis plant to the cluster avoids or lowers the need of importing low-pressure and medium-pressure steam (LPS) in this case study. Note that there is a limit to this benefit as the two additional pyrolysis plants do not further lowered the total import of steam to the cluster, as steam is also required at a different cluster site than the plastic pyrolysis plants. As indicated previously, steam is not exchanged between the different cluster sites due to the large distance between them.

3.2. Limited plastic waste

To finally illustrate the potential insights that can be obtained from the model, the impact of limited availability of plastic waste was analyzed. To do so, we limited it to a maximum of 5000 ktonne/y. The capacity flexibility was set at 10 % and all the other model parameters were kept identical to the other runs. The case study with limited available plastic was solved using the single-step method where all ACS-based processes are available to be selected by the model from the start.

Results are shown in Fig. 9, with Fig. 9a depicting the Pareto front, Fig. 9b the product distribution, Fig. 9c the carbon feedstock composition, and Fig. 9d the imported energy. The Pareto front in Fig. 9a shows a

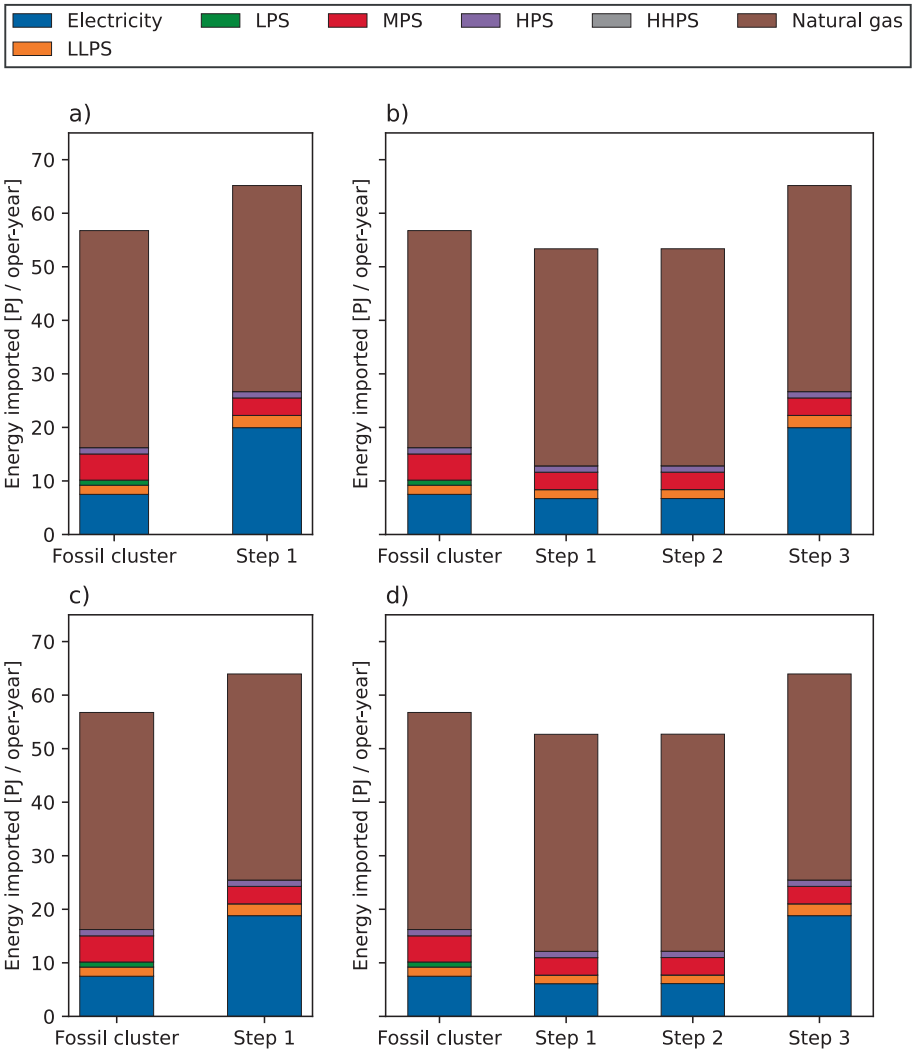

Fig. 8. The distribution of the additional steam and electricity that needs to be imported for the different model runs at their different levels of defossilization. a) Single-step at 10% flexibility. b) Multi-step at 10% flexibility. c) Single-step at 50% flexibility. d) Multi-step at 50% flexibility.

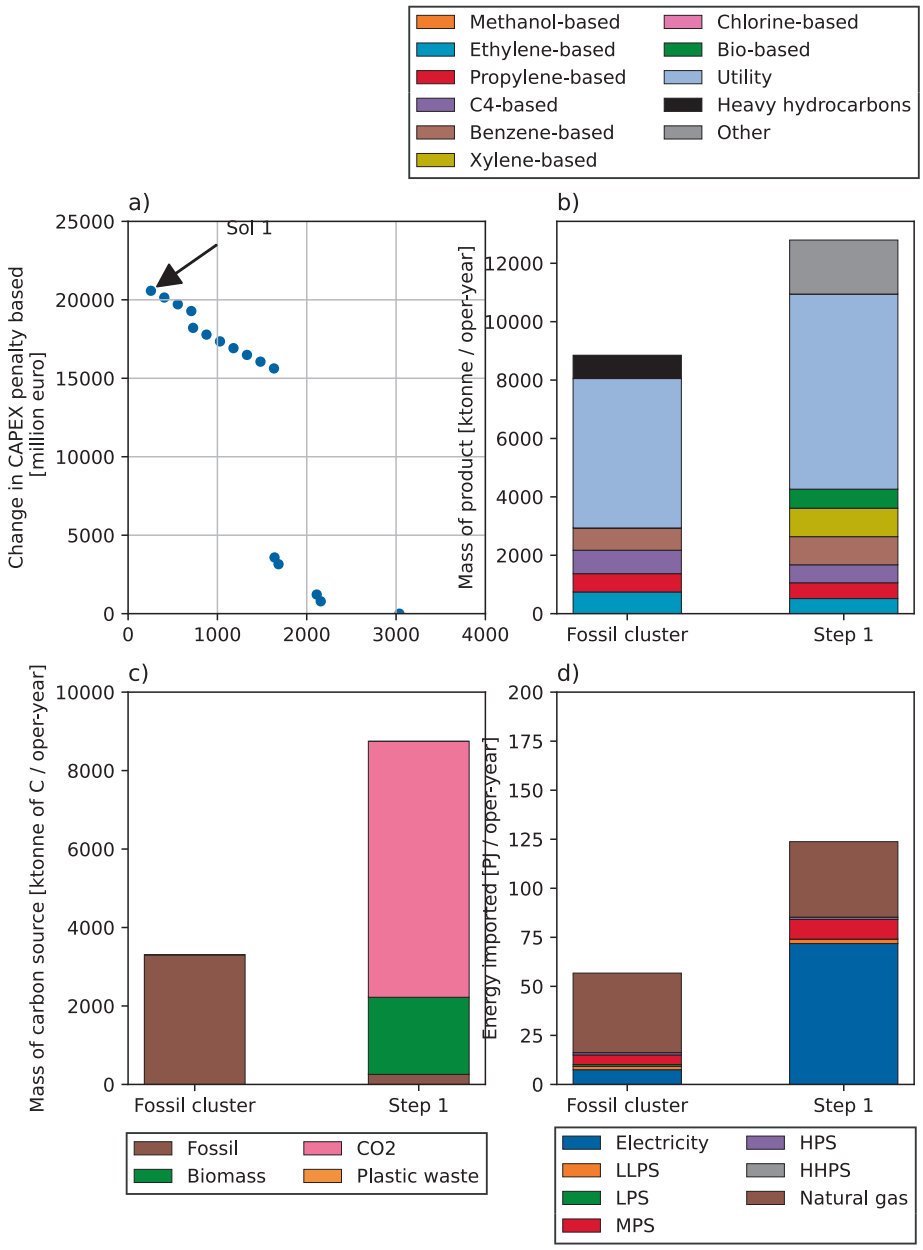

Fig. 9. Results of the model with limited availability of plastic. a) The Pareto front and selected solution. b) The product distribution for the fossil-based cluster and defossilized cluster. c) The carbon feedstock composition of the fossil-based cluster and the defossilized cluster. d) The distribution of the additional steam and electricity that needs to be imported. d Pareto front of the model run.).

very different picture compared to the other results where the plastic waste was not limited. Plastic waste can only partially defossilize the carbon feedstock, which is highlighted in the bottom part of the Pareto. This is followed by a large increase in costs to reach defosilization (4 times compared to a case without limitation in feedstock availability) as they require multiple new processes to replace the olefins plant, thereby increasing both the investment and the penalty due to stranded assets.

The processes and the respective operating capacities in the selected configurations are displayed in Table A.3. in the appendices. Note that in the case of limited availability (Fig. 9c), CO_2 is selected as the main carbon feedstock, with biomass also being selected as a secondary carbon feedstock source, and the natural gas used by the SMR plant being the only fossil-based carbon feedstock. When looking at the product distribution (Fig. 9b), the total mass of products is much smaller in comparison to the other runs. In these runs, there was a large contribution of side-products from the plastic pyrolysis plants, which are now missing due to the absence of the pyrolysis plants. Additionally, the utility and other product categories have expanded compared to the other runs. For the utility product category, this is a result of the decrease in oxygen usage for the resulting configuration, while for the other category, the MTA process produces ethane and propane as byproducts.

4. Conclusion

This paper presents a framework for modeling optimal defossilization pathways for existing petrochemical clusters by introducing alternative carbon sources. The model uses a multi-step multi-objective method, starting with an existing cluster, and uses step-wise addition of novel processes and can lock-out future choices due to past investments. For the material layer, the level of detail goes down to the composition of each stream, while for the energy layer, energy is included per type of

utility. The model selects a combination of fossil-based and ACS-based processes and feedstocks to match the production rate of end-of-value chain chemicals present in the existing petrochemical cluster while minimizing the use of fossil-based carbon feedstocks and minimizing changes to the petrochemical cluster. This allows the model to consider existing processes and their interconnections during the transformation of the cluster. Furthermore, the multi-step implementation allows to consider how petrochemical clusters are transformed over time. This is implemented in the model by increasing the design space of ACS-based processes with increasing model steps while considering the already removed fossil-based processes and constructed ACS-based in earlier steps.

The method was demonstrated using a case study based on the Port of Rotterdam petrochemical cluster. This case study included ten chemical processes that are used for the production of four end-of-value chain chemicals, five ACS-based processes providing alternative routes for producing chemical building blocks, and one ACS-based route providing an alternative route to an end-of-value chain chemical. The results of the case study showed that the model is able to select optimal combinations of processes and feedstocks to minimize fossil-based carbon. The result allow to explore the potential impact of these changes on carbon feedstocks, the product distribution and the energy imported by the cluster. In combination with the multi-step implementation, the model provides insights into the type of feedstocks that are used, the technologies that are deployed, the importance of feedstock availability and capacity flexibility, and the changes in the utility system.

This method also has limitations. The model is not a true dynamic representation of how a petrochemical cluster will transform over time. Instead, it assumes that always the most optimal configuration for the full cluster will be selected by stakeholders, thereby disregarding that companies optimize for their solution rather than the full system. This constraint is inherent to all MILP models. Nonetheless, the results of this model could be used to discuss with stakeholders or could be connected to participatory models (e.g., agent-based models). For instance, the agents of an agent-based model could make investment decisions for each company based on the solutions provided by the superstructure-based optimization model. An additional limitation, is that the optimal solution for each step is currently decided by TOPSIS. As an alternative, a decision maker could be allowed to select the optimal solution after the solutions have been ranked by TOPSIS. Additionally, the framework is currently not capable of dealing with policy changes, such as subsidy schemes and carbon pricing, and this could be introduced in future work. Furthermore, in the objective function tested in the article, the CAPEX was assumed to be completely representative of the costs associated with the loss of a fossil-based process asset, whereas in fact, the actual value of any asset decreases over time. Therefore, the penalty assigned in the model to removing fossil-based processes may overestimate the penalty. In future work introducing salvage values into the objective function could be explored.

Finally, the optimization model can be extended. Different objective functions can be implemented in the model, for example, minimizing global warming potential, water consumption use or any other environmental indicator. These alternative objective functions would however require additional input parameters. Decarbonization options for the production of utilities could also be included in the model, to investigate the impacts on the cluster. In future work, the methodology will be improved by including the physical distance between process sites and assessing the extent at which limitations in feedstock and land space availability affect the pathways. Furthermore, the presented case study will be extended to include a more complete representation of the Port of Rotterdam petrochemical cluster to cover 33 fossil-based processes.

CRediT authorship contribution statement

Michael Tan: Writing – original draft, Visualization, Software, Methodology, Investigation, Formal analysis, Data curation. **Igor Nikolic:** Writing – review & editing, Supervision, Methodology, Conceptualization. **Andrea Ramírez Ramírez:** Writing – review & editing, Supervision, Methodology, Conceptualization, Funding acquisition.

Funding

This publication is part of the project Unravelling the impacts of using alternative raw materials in industrial clusters (with project number VI.C.183.010) of the research programme Vici DO which is financed by the Dutch Research Council (NWO).

Declaration of competing interest

The authors declare that they have no known competing financial interests or personal relationships that could have appeared to influence the work reported in this paper.

Acknowledgements

The authors would like to thank Tonny Manalal, Inna Stepchuk, Paola Ibarra-González and Mar Perez-Fortes for contributing to the in-house model development.

Appendix

Table A.1
Production capacity and underlying data of all chemical processes in the model.

ID.	Process.	Capacity, kt/y.	DOI.
Fossil-based Processes.			
E1.	Ethylene Oxide (EO)	200.	https://doi.org/10.5281/zenodo.14833785.
E2.	Ethylbenzene (EB)	758.	https://doi.org/10.5281/zenodo.14910309.
E3.	Ethylene Glycol (MEG)	113.	https://doi.org/10.5281/zenodo.14833785.
M6.1.	Isobutene.	358.	https://doi.org/10.5281/zenodo.14825922.
M6.	Methyl tert-butyl ether (MTBE)	400.	
O1.	Olefins.	3,000 (Naphtha)	https://doi.org/10.5281/zenodo.14825234.
P1.1.	C_4 isomerization.	549.	https://doi.org/10.5281/zenodo.14825844.
P1.	Propylene Oxide /Tert-butyl Alcohol (PO/TBA)	250 (PO) / 603 (TBA)	
P3.	Propylene Glycol Methyl Ether (PGME)	90.	https://doi.org/10.5281/zenodo.14906547.
P6.	Propylene Oxide / Styrene Monomer (PO/SM)	650 (SM) / 290 (PO)	https://doi.org/10.5281/zenodo.14906685.
U1.	Steam Methane Reforming (SMR)	100 (H_2)	https://doi.org/10.5281/zenodo.15205929.

(*continued on next page*)

Table A.1 (*continued*)

ID.	Process.	Capacity, kt/y.	DOI.
U2.	Air Separation Unit (ASU)	7,560 (Air)	https://doi.org/10.5281/zenodo.15205968.
U6.	Waste-fired boiler (WFB)	1,671 (LLPS)	https://doi.org/10.5281/zenodo.14825977.
Deployed ACS-based Processes.			
BM6.1.	Bio-Isobutene.	358.	https://doi.org/10.5281/zenodo.14826089.
CM1.	CO_2 to methanol.	406.	https://doi.org/10.5281/zenodo.14894463.
CO1.	Direct electrochemical reduction of CO_2 to ethylene.	329.	https://doi.org/10.5281/zenodo.14894342.
MA1.	Methanol to aromatics.	535 (Benzene)972 (p-Xylene) 68 (Propylene) 21 (Ethylene)	https://doi.org/10.5281/zenodo.14894482.
MO1.	Methanol to olefins.	314 (Ethylene) 398 (Propylene) 60 (Benzene)	https://doi.org/10.5281/zenodo.14894523.
PM1.	Plastic gasification followed by methanol synthesis.	408.	https://doi.org/10.5281/zenodo.14894543.
PO1.	Plastic pyrolysis plant.	1055 (Naphtha)	https://doi.org/10.5281/zenodo.14894590.

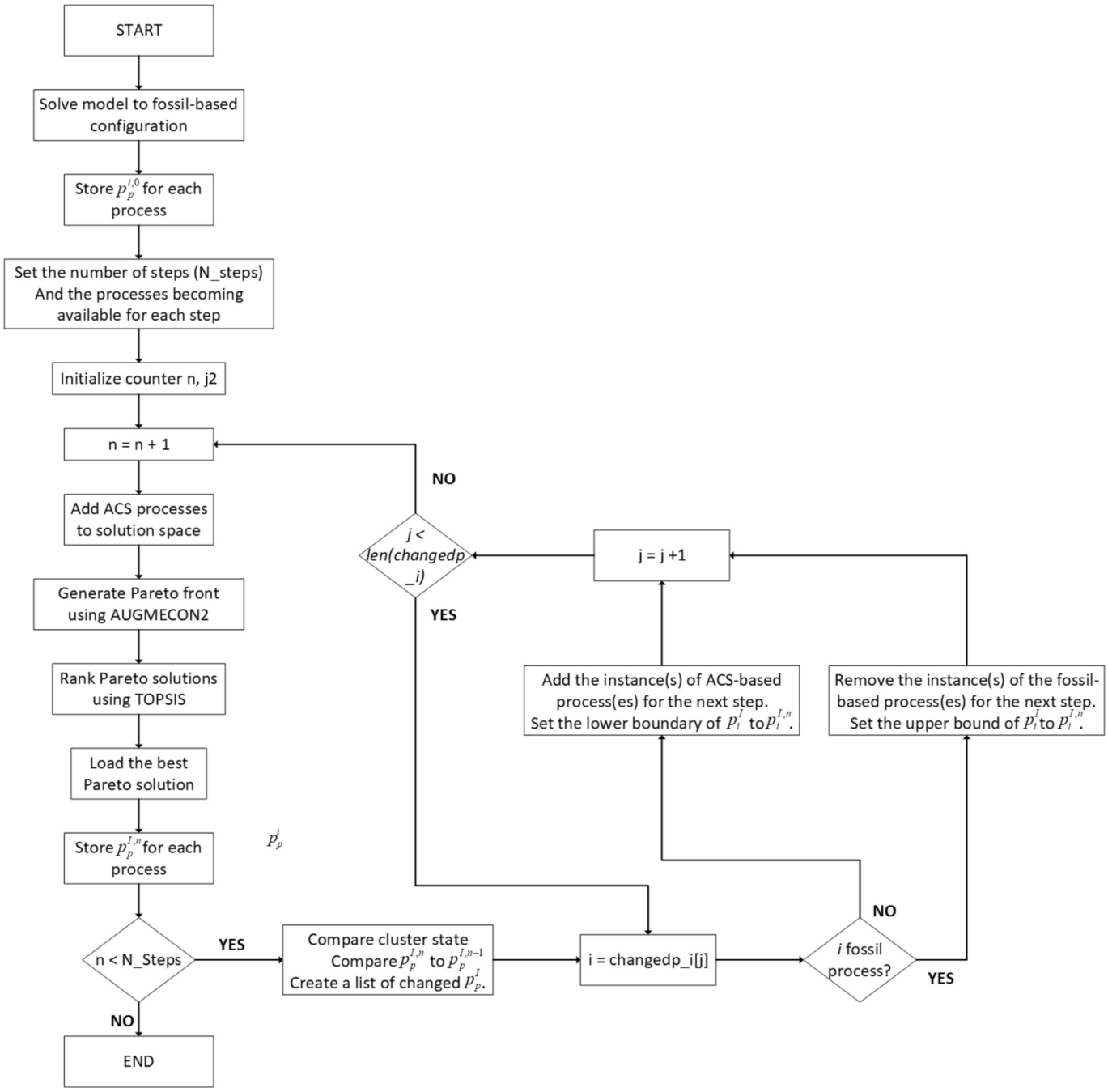

Fig. A.1. . Flowchart for the multi-step multi-objective method

Table A.2
Selected processes and their operating capacities.

	Run A.		Run B.		Run C.		Run D.	
Node.	p^I	Operating capacity.	p^I	Operating capacity.	p^I	Operating capacity.	p^I	Operating capacity.
E1.	1.	100 %	1.	100 %	1.	100 %	1.	100 %
E2.	1.	100 %	1.	100 %	1.	100 %	1.	100 %
E3.	1.	100 %	1.	100 %	1.	100 %	1.	100 %
M61.	0.	–	0.	–	0.	–	0.	
M6.	1.	100 %	1.	100 %	1.	100 %	1.	100 %
O1.	1.	94.2 %	1.	94.2 %	1.	85.6 %	1.	85.6 %
P11.	0.	–	0.	–	0.	–	0.	–
P1.	0.	–	0.	–	0.	–	0.	–
P3.	1.	100 %	1.	100 %	1.	100 %	1.	100 %
P6.	1.	100 %	1.	100 %	1.	100 %	1.	100 %
U1.	1.	90.0 %	1.	90.0 %	1.	53.1 %	1.	53.1 %
U2.	1.	94 %	1.	94.9 %	1.	71.6 %	1.	71.6 %
U3-IS.	1.	100 %	1.	100 %	1.	100 %	1.	100 %
U3-SL.	1.	100 %	1.	100 %	1.	100 %	1.	100 %
U6-A.	1.	100 %	1.	100 %	1.	100 %	1.	100 %
U6-I1.	0.	–	0.	–	0.	–	0.	–
U6-I2.	0.	–	0.	–	0.	–	0.	–
BM61.	1.	–	1.	–	1.	–	1.	–
CM1.	0.	–	0.	–	0.	–	0.	–
CO1.	0.	–	0.	–	0.	–	0.	–
MA1.	0.	–	0.	–	0.	–	0.	–
MO1.	0.	–	0.	–	0.	–	0.	–
PO1.	3.	–	3.	–	3.	–	1.	–

Table A.3
Selected processes and operation capacities when plastic feedstock is limited.

	Run A.	
Node.	p^I	Operating capacity.
E1.	1.	100 %
E2.	1.	100 %
E3.	1.	100 %
M61.	0.	–
M6.	1.	100 %
O1.	0.	–
P11.	0.	–
P1.	0.	–
P3.	1.	100 %
P6.	1.	100 %
U1.	1.	100 %
U2.	1.	94.9 %
U3-IS.	1.	100 %
U3-SL.	1.	100 %
U6-A.	1.	100 %
U6-I1.	0.	–
U6-I2.	0.	–
BM61.	1.	–
CM1.	28.	–
CO1.	1.	–
MA1.	1.	–
MO1.	1.	–
PO1.	3.	–

Data availability

The data respositories for the underlying process data is provided in Table A.1. of the appendices, the software implementation is provided on https://doi.org/10.5281/zenodo.17079434

References

Bishnu, S., Linke, P., Alnouri, S., El-Halwagi, M., 2017. Multi-Period Water Network Synthesis for Eco Industrial Parks considering Regeneration and Reuse. Chem. Prod. Process Model. 12. https://doi.org/10.1515/cppm-2016-0049.

Boix, M., Montastruc, L., Azzaro-Pantel, C., Domenech, S., 2015. Optimization methods applied to the design of eco-industrial parks: a literature review. J. Clean. Prod. 87, 303–317. https://doi.org/10.1016/j.jclepro.2014.09.032.

Bynum, M.L., Hackebeil, G.A., Hart, W.E., Laird, C.D., Nicholson, B.L., Siirola, J.D., Watson, J.-P., Woodruff, D.L., 2021. Pyomo — Optimization Modeling in Python. Springer International Publishing, Cham.

Granacher, J., Van, N.T., Castro-Amoedo, R., Maréchal, F., 2022. Overcoming decision paralysis—A digital twin for decision making in energy system design. Appl. Energy 306, 117954. https://doi.org/10.1016/j.apenergy.2021.117954.

Gurobi Optimization (2024) Gurobi Optimizer Reference Manual.

Han, R., Kang, L., Jiang, Y., Wang, J., Liu, Y., 2020. Optimization of an inter-plant hydrogen network: a simultaneous approach to solving multi-period optimization problems. Processes 8, 1–19. https://doi.org/10.3390/pr8121548.

Han, F., Sun, M., Jia, X., Klemeš, J.J., Shi, F., Yang, D., 2022. Agent-based model for simulation of the sustainability revolution in eco-industrial parks. Environ. Sci. Pollut. Res. 29, 23117–23128. https://doi.org/10.1007/s11356-021-17503-5.

Hart, W.E., Watson, J.-P., Woodruff, D.L., 2011. Pyomo: modeling and solving mathematical programs in Python. Math. Program. Comput. 3, 219–260. https://doi.org/10.1007/s12532-011-0026-8.

Hwang, C.-L., Yoon, K., 1981. Multiple Attribute Decision making. Springer, Berlin Heidelberg, Berlin, Heidelberg.

Kantor, I., Betancourt, A., Elkamel, A., Fowler, M., Almansoori, A., 2015. Generalized mixed-integer nonlinear programming modeling of eco-industrial networks to reduce cost and emissions. J. Clean. Prod. 99, 160–176. https://doi.org/10.1016/j.jclepro.2015.03.017.

Kantor, I., Robineau, J.L., Bütün, H., Maréchal, F., 2020. A Mixed-Integer Linear programming Formulation for Optimizing Multi-Scale Material and Energy Integration. Front. Energy Res. 8. https://doi.org/10.3389/fenrg.2020.00049.

Kim, H., Lee, B., Lim, D., Choe, C., Lim, H., 2021. What is the best green propylene production pathway?: Technical, economic, and environmental assessment. Green Chem. 23, 7635–7645. https://doi.org/10.1039/d1gc01791h.

Kim, S.H., Yoon, S.G., Chae, S.H., Park, S., 2010. Economic and environmental optimization of a multi-site utility network for an industrial complex. J. Environ. Manage. 91, 690–705. https://doi.org/10.1016/j.jenvman.2009.09.033.

Kuo, C.C., Chang, C.T., 2014. Improved model formulations for multiperiod hydrogen network designs. Ind. Eng. Chem. Res. 53, 20204–20222. https://doi.org/10.1021/ie5037726.

Liptow, C., Tillman, A.M., Janssen, M., 2015. Life cycle assessment of biomass-based ethylene production in Sweden — is gasification or fermentation the environmentally preferable route? Int. J. Life Cycle Assess. 20, 632–644. https://doi.org/10.1007/s11367-015-0855-1.

Manalal, J.T., Pérez-Fortes, M., Ramírez, A., 2025. Re-wiring petrochemical clusters: impact of using alternative carbon sources for ethylene production. Green Chem. 27, 6641–6659. https://doi.org/10.1039/D4GC06042C.

Martelli, E., Elsido, C., Mian, A., Marechal, F., 2017. MINLP model and two-stage algorithm for the simultaneous synthesis of heat exchanger networks, utility systems and heat recovery cycles. Comput. Chem. Eng. 106, 663–689. https://doi.org/10.1016/j.compchemeng.2017.01.043.

Mavrotas, G., 2009. Effective implementation of the ε-constraint method in Multi-Objective Mathematical programming problems. Appl. Math Comput. 213, 455–465. https://doi.org/10.1016/j.amc.2009.03.037.

Mavrotas, G., Florios, K., 2013. An improved version of the augmented s-constraint method (AUGMECON2) for finding the exact pareto set in multi-objective integer programming problems. Appl. Math Comput. 219, 9652–9669. https://doi.org/10.1016/j.amc.2013.03.002.

Mencarelli, L., Chen, Q., Pagot, A., Grossmann, I.E., 2020. A review on superstructure optimization approaches in process system engineering. Comput. Chem. Eng. 136. https://doi.org/10.1016/j.compchemeng.2020.106808.

Meng, F., Wagner, A., Kremer, A.B., Kanazawa, D., Leung, J.J., Goult, P., Guan, M., Herrmann, S., Speelman, E., Sauter, P., Lingeswaran, S., Stuchtey, M.M., Hansen, K., Masanet, E., Serrenho, A.C., Ishii, N., Kikuchi, Y., Cullen, J.M., 2023. Planet-compatible pathways for transitioning the chemical industry. Proc. Natl. Acad. Sci. 120, 2017. https://doi.org/10.1073/pnas.2218294120.

Pan, M., Sikorski, J., Akroyd, J., Mosbach, S., Lau, R., Kraft, M., 2016. Design technologies for eco-industrial parks: from unit operations to processes, plants and industrial networks. Appl. Energy 175, 305–323. https://doi.org/10.1016/j.apenergy.2016.05.019.

Tan, M., Ibarra-González, P., Nikolic, I., Ramírez Ramírez, A., 2024. Understanding the Level of Integration in existing Chemical Clusters: Case Study in the Port of Rotterdam. Circular Economy and Sustainability. https://doi.org/10.1007/s43615-024-00410-5.

Valenzuela-Venegas, G., Vera-Hofmann, G., Díaz-Alvarado, F.A., 2020. Design of sustainable and resilient eco-industrial parks: Planning the flows integration network through multi-objective optimization. J. Clean. Prod. 243. https://doi.org/10.1016/j.jclepro.2019.118610.

Vogt;, E.T.C., Weckhuysen, B.M., 2024. The refinery of the future. Nature 629, 295–306. https://doi.org/10.1038/s41586-024-07322-2.

Zuiderveen, E.A.R., Caldeira, C., Vries, T., Schenk, N.J., Huijbregts, M.A.J., Sala, S., Hanssen, S.V., van Zelm, R., 2024. Evaluating the Environmental Sustainability of Alternative Ways to produce Benzene, Toluene, and Xylene. ACS Sustain. Chem. Eng. 12, 5092–5104. https://doi.org/10.1021/acssuschemeng.3c06996.